

Article

Description of Dynamic Recrystallization by Means of An Advanced Statistical Multilevel Model: Grain Structure Evolution Analysis

Peter Trusov , Nikita Kondratev  and Andrej Podsedertsev

Laboratory of Multilevel Structural and Functional Materials Modeling, Perm National Research Polytechnic University, 614990 Perm, Russia; kondratevns@gmail.com (N.K.); stevenmoore@yandex.ru (A.P.)

* Correspondence: tpv@matmod.pstu.ac.ru

Abstract: Physical multilevel models of inelastic deformation that take into account the material structure evolution hold promise for the development of functional materials. In this paper, we propose an advanced (modified via analyzing the mutual arrangement of crystallites) statistical multilevel model for studying thermomechanical processing of polycrystals that includes a description of the dynamic recrystallization process. The model is based on the consideration of homogeneous elements (grains, subgrains) aggregated into a representative volume (macropoint) under the Voigt hypothesis. In the framework of this statistical approach, there is no mandatory requirement for continuous filling of the computational domain with crystallites; however, the material grain structure cannot be created arbitrarily. Using the Laguerre polyhedra, we develop a method of grain structure simulation coupled with subsequent processing and transferring of the necessary data on the grain structure to the modified statistical model. Our research is of much current interest due to the fact that the mutual arrangement of crystallites, as well as the interfaces between them, has a significant impact on the properties of polycrystals, which are particularly important for physical mechanisms that provide and accompany the processes of inelastic deformation (recrystallization, grain boundary hardening, grain boundary sliding, etc.). The results of the simulations of the high-temperature deformation of a copper polycrystal, including the description of the recrystallization process, are presented.

Keywords: multilevel models; dynamic recrystallization; grain shape and grain size; defect and grain structure evolution



Citation: Trusov, P.; Kondratev, N.; Podsedertsev, A. Description of Dynamic Recrystallization by Means of An Advanced Statistical Multilevel Model: Grain Structure Evolution Analysis. *Crystals* **2022**, *12*, 653. <https://doi.org/10.3390/cryst12050653>

Academic Editor: Zheng Mingyi

Received: 31 March 2022

Accepted: 29 April 2022

Published: 2 May 2022

Publisher's Note: MDPI stays neutral with regard to jurisdictional claims in published maps and institutional affiliations.



Copyright: © 2022 by the authors. Licensee MDPI, Basel, Switzerland. This article is an open access article distributed under the terms and conditions of the Creative Commons Attribution (CC BY) license (<https://creativecommons.org/licenses/by/4.0/>).

1. Introduction

Methods for processing polycrystalline materials, especially hard-to-deform alloys, via severe plastic deformation (stamping, drawing, extrusion, forging, etc.) usually include high homologous temperatures [1,2]. An actual problem that manufacturers face during this processing is to obtain structures and products with optimal mechanical properties (high strength, high yield strength, low weight, etc.) [3,4]. Plastic deformation in these processes is usually accompanied by the appearance and evolution of structural defects at various structural-scale levels, which in turn causes inhomogeneity of the physical and mechanical properties [5,6]. The high temperature of the plastic deformation process and subsequent heating reduce the number of defects and promote their redistribution, increasing the uniformity of the structure. This is possible due to the implementation of a combination of two high-temperature processes, namely dynamic recovery (DRV) and dynamic recrystallization (DRX) [5,7–10]. DRV is followed by reduction and redistribution of defects (primarily, dislocations) and densities, which usually results in the formation of subgrain, block–cellular, and cellular structures [5,7,8,11]. DRX refers to the formation and further development of new, less-defective grains by absorbing neighboring grains [5,7,8]. If this process is implemented in the material in a heterogeneous way, where the stages of formation of DRX nuclei and their subsequent growth are clearly separated, then it is

called discontinuous dynamic recrystallization (DDRX) [5] or classical DRX [7]. However, if the DRX process occurs homogeneously in such a way that the stages of formation and growth of new grains are not clearly distinguished, then it is called continuous dynamic recrystallization (CDRX) [5,7]. The main material characteristic of the development of a grain and defect structure during DRX and its type is the stacking fault energy (SFE). The increased SFE values promote the formation of a subgrain structure under active recovery effects, and accordingly the implementation of CDRX, while the lower SFE values are responsible for the occurrence of DDRX [5,7].

At present, the multilevel models of inelastic deformation with internal variables are widely used to simulate changes in the structure and responses of the materials [6,12–16]. There are three classes of multilevel models: statistical, direct, and self-consistent. Statistical models consider a representative macrovolume of a material (“macropoint”) as a set of individual grains combined into a polycrystalline aggregate, as hypothesized by Voigt, Reiss, and Kroener [17–19]. Self-consistent (mean-field) models are based on solving the boundary single inclusion problem of a crystallite (grain, subgrain, fragment) embedded in a matrix by imaging the averaged (effective) characteristics of a polycrystal [20–22]. Direct models rely on solving boundary value problems and on determining the field values of the model (stresses, strains, and internal variables) for each crystallite included in the representative macrovolume under consideration [13,23,24]. Statistical models have been recognized by many authors as the least accurate among all three classes of models, yet their modifications make it possible to explicitly consider the current state of neighboring grains by highlighting their contact interactions along the conjugate flat sections of boundaries (facets) of grains [25,26]. Additionally, these models have high computational efficiency [27]. One of the main drawbacks of the self-consistent models is that they are unable to take into account real physical interactions between the neighboring crystallites (e.g., exchange of dislocation flows, formation of orientation misfit dislocations) and require the replacement of the environment by a continuum with averaged properties, which do not reflect the real state of the grain and defect structures. Direct models are known to be the most accurate models, yet they remain the most resource-intensive [28]. The implementation of direct models of crystallites with varying compositions and moving boundaries involves great computational difficulties, especially when studying a wider range of physical processes, including solid-state phase transitions and recrystallization processes.

Numerous approaches and methods have been developed to model DRX [5,29,30]. Phenomenological models are the most simplified models, which include an empirical or semi-empirical description of a recrystallized material fraction. The Johnson–Mehl–Avrami–Kolmogorov (JMAK) kinetic equations form the basis for describing the evolution of the recrystallized volume fraction of polycrystals in these models [31–33]. The development of this approach is associated with creating models able to describe such characteristics of the grain structure, as the grain size, grain shape, and grain boundary orientation [34–36]. The JMAK equations often turn out to be insufficient for studying the grain structure evolution because they do not take into account the heterogeneous nature of the DRX process and are only applicable within a narrow range of variation in the initial structure, temperature, strain, and strain rate [37,38]. Recent developments in the computer technology provide an opportunity to develop physical approaches that permit an explicit description of the grain structure evolution [5,6]. In the framework of this class of models, internal variables and parameters are introduced to characterize the material structure and to assess factors responsible for the formation of DRX nuclei and for the migration of grain boundaries. Due to this, these models are applied to describe the formation of the required material structure, and they are well suited to technological regimes in the metallurgical and manufacturing industries. Within this physical approach, there are several types of models that include descriptions of dynamic recrystallization, in particular self-consistent [8,21,39,40] and direct [41–43] models. One of the main problems encountered in modeling DRX processes is the description of the grain structure evolution that occurs due to the formation of new grains and due to the migration of their high-angle boundaries. To describe the grain

structure evolution by applying the models of the above type, various approaches are typically used, including the Monte Carlo method [44], cellular automaton method [38,45,46], phase-field method [47], level set method [43,48], graph theory based methods [49,50], and some others.

Despite the great number of approaches and methods, the problem of modeling the grain structure evolution during DRX still remains an urgent research issue and requires further research. Recent papers [8,38,40,43] are indicative of a current interest in this subject. The topicality of the problem is also related to the presence of a relationship between the current state of the grain structure and the macro-properties of polycrystals. This fact has been repeatedly confirmed by the results of many independent experiments [5,51,52]. The most well-known manifestation of the influence of the state of the grain structure on the properties of the material is the dependence of the yield strength on the average grain size (Hall–Petch equation) [53–55]. Severe hot plastic deformation produces significant changes (usually refinement) in the grain structure, which are mainly associated with DRX [5,7]. The grain structure determined by the shape and size of crystallites is of decisive importance in providing effective mechanical properties (plasticity, creep, hardness, fatigue, etc.) of a polycrystalline material [56,57]. As an example, the formation of equiaxed grains and their refinement during recrystallization facilitate the implementation of grain boundary sliding, and consequently the initiation of deformation in the structural superplasticity mode under appropriate temperature and velocity conditions [26,58]. This causes abnormally large deformations to appear at almost constant and relatively low values of plastic flow stress.

In view of the foregoing, the problem of developing an advanced constitutive physical model of a polycrystalline material relying on an explicit physical description of the DRX process needed to analyze the evolution of grain and defect structures is of particular importance. In this paper, we propose an original method of statistical modeling to form and reconstruct the grain structure by applying Laguerre polyhedra [59]. The developed geometric model for describing the grain shape and grain size allows one to overcome the above-mentioned difficulties inherent in using self-consistent and direct models. It has high computational efficiency and is able to describe the peculiarities of physical mechanisms, where the decisive factor is the interaction between contacting grains.

Section 2 presents the structure, scale levels, and relationships of an advanced statistical multilevel model for describing inelastic deformation with allowance for the DDRX and the mechanism governing the formation of nuclei and their development into individual low-defect grains. Section 3 discusses a method for grain structure formation and reconstruction during high-temperature deformation using the Laguerre polyhedra, as well as subsequent processing and transfer of the obtained data on the grain structure to the advanced statistical model. Section 4 gives a description and analysis of the obtained results.

2. The Advanced Statistical Multilevel Model for Describing Inelastic Deformation during Discontinuous Dynamic Recrystallization

This study investigates DDRX, which is a common phenomenon encountered in plastic formation of a wide class of polycrystalline materials with medium and low SFE values, including copper, nickel, austenitic steels, and some aluminum alloys [5,7]. At the initial stage of hot plastic deformation, DDRX is characterized by the formation of low-defect nuclei, which absorb the neighboring more-defective grains due to boundary migration. Thus, two processes are responsible for the occurrence of DDRX: (1) the formation of nuclei and their further development into new grains; (2) the migration of the high-angle boundaries of DRX grains [5,7]. DRX nuclei have a characteristic size of the order of a micrometer and are not formed due to random fluctuations, as in the case of phase transitions [5]. They appear in the course of directed rearrangement of defect and subgrain structures. For most metals, the commonly accepted mechanism of nuclei formation during DDRX involves the movement (“bending”, “swelling”) of the grain boundary regions associated with the original subgrains of a polycrystal [60–63]. This mechanism,

first investigated for static recrystallization, was described in [64]. The presence of this phenomenon during DDRX was confirmed by the theoretical and experimental results of many researchers [60,61,63,65]. The development of the DDRX process governed by this mechanism is presented schematically in Figure 1. Initially, the first nuclei layer is formed at the original grain boundaries, and it has orientation coherency with the parent grain (Figure 1b). In a similar way, new grains (their average size decreases gradually) are formed at the boundaries of previously recrystallized grains (Figure 1c,d). These grains occur due to the addition of atoms to a subgrain (a DRX nucleus) along the grain boundaries and due to their subsequent penetration deep into the defective grain. In Figure 1, the following designations are used: ε_c is the critical deformation up to which no DRX occurs; ε_m is the deformation corresponding to the maximum value of stresses σ_m in the load diagram; ε_s is the deformation corresponding to almost complete recrystallization of the material; ε_x is the deformation corresponding to one recrystallization cycle ($\varepsilon_s = \varepsilon_c + \varepsilon_x$).

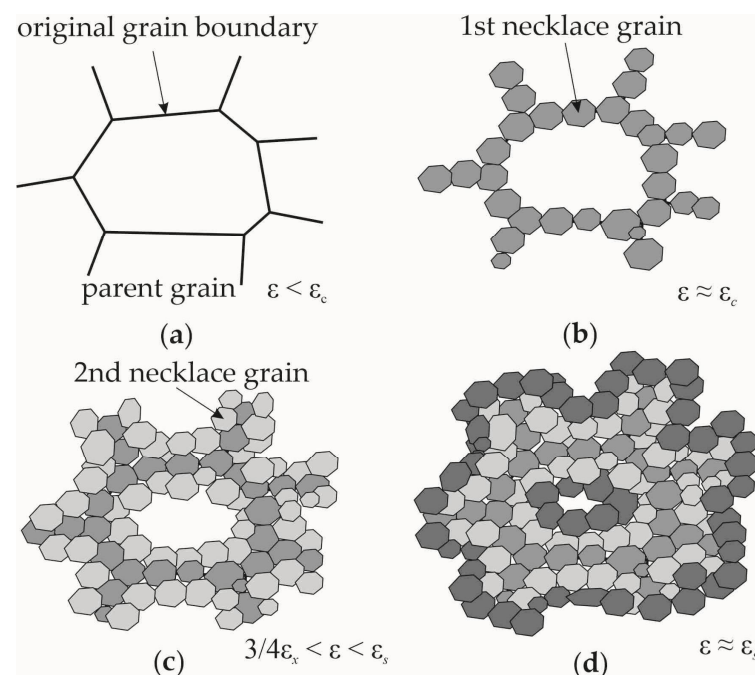


Figure 1. Scheme for the formation of a fine-grained structure during DDRX at various degrees of deformation ε : $\varepsilon < \varepsilon_c$ (a), $\varepsilon \approx \varepsilon_c$ (b), $3/4\varepsilon_x < \varepsilon < \varepsilon_s$ (c), $\varepsilon \approx \varepsilon_s$ (d) (it was developed based on [61]).

Previously, the authors developed an advanced statistical multilevel model intended for describing static [25] and dynamic recrystallization [66,67]. In these papers, the processes of preliminary plastic deformation and the subsequent annealing of the material or its deformation at a given temperature were investigated to evaluate the initial stage of recrystallization. The present article provides a description of a significantly modified model in regard to refining the simulation of the polycrystal grain structure evolution. The model is designed to study the processes of severe plastic deformation of polycrystalline materials at elevated temperatures of inelastic deformation.

In solving the formulated problem, we distinguish three structural levels in the structure of a statistical multilevel model. They are the macrolevel, mesolevel-I, and mesolevel-II. At the macrolevel, the statistical description of a representative number of grains with uniform distribution of orientations of crystallographic axes in the space of the reference configuration is carried out. At mesolevel-I, the behavior of a separate grain consisting of mesolevel-II elements (homogeneous subgrains) is investigated. The grains are separated by high-angle boundaries, whose misorientation is greater than 10–15 degrees; the subgrain misorientation is about several degrees, and as a rule it increases with increasing

inelastic deformation [5,68]. A scheme illustrating the relationship between the scale-based submodels is shown in Figure 2.

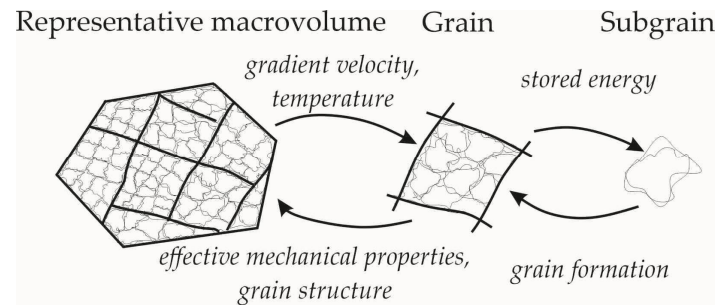


Figure 2. Scale levels and the connection between the structural elements of a multilevel model (thin lines correspond to subgrain boundaries, bold lines show grains boundaries).

At the macrolevel, the effective properties of the material are determined and the impacts are transferred from this level to the underlying scale levels. For each moment of time t , the mechanical and thermal effects are prescribed and the velocity gradient $\hat{\nabla}\mathbf{V}(t)$ and temperature $\Theta(t)$ are assumed to be known at the macrolevel. Therefore, for each grain, the following equality is true [6]:

$$\hat{\nabla}\mathbf{v}(t) = \hat{\nabla}\mathbf{V}(t), \theta(t) = \Theta(t), \quad (1)$$

where $\hat{\nabla}\mathbf{v}(t)$ is the velocity gradient of the grain's material particle; $\theta(t)$ is the grain temperature; $\hat{\nabla}$ is the Hamilton operator in the current Lagrangian coordinate system; \mathbf{V} , \mathbf{v} are the velocity vectors obtained at macro and mesolevels. The indexes denoting the grain (subgrain) number are omitted hereinafter, unless otherwise specified.

At mesolevel-I, the problem of determining the stress–strain state of a grain and the corresponding internal variables of the model is solved using an advanced statistical model. The mathematical formulation of a mesolevel-I model contains the following relations [66,67]:

$$\boldsymbol{\kappa}^{cr} = \Pi : \left(\hat{\nabla}\mathbf{v}^T - \boldsymbol{\omega} - \mathbf{z}^{in} \right), \quad (2)$$

$$\mathbf{z}^{in} = \sum_{k=1}^K \dot{\gamma}^{(k)} \mathbf{b}^{(k)} \mathbf{n}^{(k)}, \quad (3)$$

$$\boldsymbol{\tau}^{(k)} = \mathbf{b}^{(k)} \mathbf{n}^{(k)} : \boldsymbol{\kappa}, \quad (4)$$

$$\dot{\gamma}^{(k)} = \dot{\gamma}_0 \left(\frac{\boldsymbol{\tau}^{(k)}}{\boldsymbol{\tau}_c^{(k)}} \right)^m H \left(\boldsymbol{\tau}^{(k)} - \boldsymbol{\tau}_c^{(k)} \right), \quad (5)$$

$$\dot{\boldsymbol{\tau}}_c^{(k)} = \dot{\boldsymbol{\tau}}_{cs}^{(k)} + \dot{\boldsymbol{\tau}}_{cgb}^{(k)}, \quad (6)$$

$$\dot{\boldsymbol{\tau}}_{cs}^{(k)} = \sum_{j=1}^{N_s} h^{(kj)} \dot{\gamma}^{(j)}, \quad (7)$$

$$h^{(kl)} = \left[q_{lat} + (1 - q_{lat}) \delta^{(kl)} \right] h^{(l)}, \quad h^{(l)} = h_0 \left| 1 - \boldsymbol{\tau}_c^{(l)} / \boldsymbol{\tau}_{sat} \right|^a, \quad (8)$$

$$\dot{\boldsymbol{\tau}}_{cgb}^{(k)} = \eta \sum_{j=1}^{N_f} \frac{S_j}{S} \sum_{s=1}^{N_s} \xi^{(s,j)} \dot{\gamma}^{(s)} \boldsymbol{\tau}_{bs}^{(k,s)}, \quad (9)$$

$$\boldsymbol{\omega} = \dot{\mathbf{o}} \cdot \mathbf{o}^T = \mathbf{I} \times (\mathbf{k}_3 \mathbf{k}_1 \mathbf{k}_2 - \mathbf{k}_2 \mathbf{k}_1 \mathbf{k}_3 + \mathbf{k}_1 \mathbf{k}_2 \mathbf{k}_3) : \mathbf{l}^e, \quad (10)$$

$$\mathbf{z}^e = \mathbf{z} - \mathbf{z}^{in}, \quad (11)$$

$$e_{st} = \frac{\alpha}{G} \left(\boldsymbol{\tau}_c^2 - \boldsymbol{\tau}_{c0}^2 \right). \quad (12)$$

The corresponding initial conditions are written as follows [6]:

$$\boldsymbol{\kappa}|_{t=0} = \boldsymbol{\kappa}_0, \quad \mathbf{o}|_{t=0} = \mathbf{o}_0, \quad \tau_{cs}^{(k)}|_{t=0} = \tau_{cs0}^{(k)}, \quad \tau_{ctw}^{(k)}|_{t=0} = \tau_{ctw0}^{(k)}, \quad \gamma_s^{(k)}|_{t=0} = \gamma_{s0}^{(k)}. \quad (13)$$

Here, $\boldsymbol{\kappa} = \frac{\rho}{\hat{\rho}} \boldsymbol{\sigma}$ is the mesolevel weighted Kirchoff stress tensor; $\boldsymbol{\kappa}^{cr} = d\boldsymbol{\kappa}/dt + \boldsymbol{\kappa} \cdot \boldsymbol{\omega} - \boldsymbol{\omega} \cdot \boldsymbol{\kappa}$ is its corotational derivative; $\boldsymbol{\sigma}$ is the mesolevel Cauchy stress tensor; $\mathbf{z} = \hat{\nabla} \mathbf{v}^T - \boldsymbol{\omega}$ is the strain measure satisfying the objectivity requirement; $\mathbf{z}^e, \mathbf{z}^{in}$ are the mesolevel elastic and inelastic components of the strain rate measure; \mathbf{l}^e is the elastic component of the transposed velocity gradient; $\rho, \hat{\rho}$ denote the material density in the reference and current configurations, respectively; $\dot{\gamma}^{(k)}$ is the shear rate on the k -th intragranular slip system; $\dot{\gamma}_0$ is the shear rate on the slip system when the tangential stress reaches the critical shear stress; m is the strain rate sensitivity exponent of the material; $\mathbf{b}^{(k)}, \mathbf{n}^{(k)}$ are the unit vectors of the slip direction and the normal to the k -th slip system, respectively; H is the Heaviside function; $\tau^{(k)}, \tau_c^{(k)}$ are the shear and critical stresses of the k -th system, respectively; $\tau_{cs}^{(k)}, \tau_{cgb}^{(k)}$ are the components of critical stresses of the k -th system, which occur due to the interactions of dislocations with the dislocation structure and grain boundaries, respectively; $\tau_c^2 = \sum_{k=1}^{N_s} (\tau_c^{(k)})^2, \tau_{c0}^2 = \sum_{k=1}^{N_s} (\tau_{c0}^{(k)})^2$ are the total squared critical stresses in the grain under study at the current and initial instants of deformation, respectively; $h^{(kl)}$ is the matrix describing the crystal hardening caused by the interactions between dislocations and forest dislocations; q_{lat} is the latent hardening parameter; τ_{sat} is the saturation stress; h_0, a are the parameters describing material hardening; N_s, N_f denote the number of slip systems and the number of facets of the considered grain, respectively; S, S_j are the grain area and the j -th grain facet, respectively; $\xi^{(s,j)}$ is the parameter characterizing the interactions between the dislocations of the s -th slip system of the considered grain and those of the neighboring grain along the j -th facet, respectively (the definition of this parameter is given in [69]); $\tau_{bs}^{(k,s)}$ is the component of the shear barrier stresses acting on the k -th slip on the side of orientation misfit dislocations that appear in the facets because of the dislocation motion on the s -th system; η is the dimensionless parameter defined during the model identification procedure; $\boldsymbol{\pi}$ is the elastic tensor of the crystallite, the components of which π^{ijmn} were defined and turned out to constant in the actual basis \mathbf{k}_i (in the reference configuration, the basis vectors are denoted by \mathbf{k}_0^i) of the rigid moving coordinate system (MCS) rotating with spin $\boldsymbol{\omega}$. The rigid orthonormal coordinate system is related to one crystallographic direction and the crystallographic plane containing this direction. In the reference configuration, the basis of the MCS coincides with the basis of the crystallographic coordinate system (CCS). The basis of the CCS is distorted during deformation, while the basis of the MCS remains rigid. The motion relative to the CCS is a deformation motion. The definition of MCS and spin is given in [70]; $\mathbf{o} = \mathbf{k}_i \mathbf{k}_0^i$ is the tensor that combines the MCS with the laboratory coordinate system (LCS); α is the dimensionless experimentally determined correction parameter characterizing the fraction of energy stored in dislocations; G is the shear modulus; $\delta^{(kl)}$ is the Kronecker delta; the dot above the corresponding mesolevel variables denotes the material time derivative t ; the subscript T denotes the transpose of the value of the second rank tensor. The transition to macrolevel variables is implemented via volume averaging of the corresponding mesolevel variables. To describe hardening by analyzing the interaction of mobile dislocations with forest dislocations (relation for $\dot{\tau}_{cs}^{(k)}$), we apply the known hardening law [71,72] and the grain boundary hardening law (relation for $\dot{\tau}_{cgb}^{(k)}$) described in [69].

At the macrolevel, we calculate the average values of stresses $\boldsymbol{\Sigma}$, elastic properties $\boldsymbol{\Pi}$, and an inelastic component of the velocity gradient $\hat{\nabla} \mathbf{v}^{in}$ [6]:

$$\boldsymbol{\Sigma} = \langle \boldsymbol{\sigma} \rangle, \quad \boldsymbol{\Pi} = \langle \boldsymbol{\pi} \rangle, \quad \hat{\nabla} \mathbf{v}^{in} = \langle \hat{\nabla} \mathbf{v}^{in} \rangle, \quad (14)$$

where $\langle \rangle$ is the volume averaging operator.

At the mesolevel-II (the level of individual subgrains), which is an auxiliary level, there is an opportunity to accurately evaluate the above DDRX recrystallization mechanism when modeling the formation of the nuclei located near the grain boundary. When the Bailey–Hirsch criterion is satisfied, the DRX nuclei start to grow, and as a result new grains are formed. According to this criterion, a decrease in local volume energy due to defect elimination must be greater or equal to an increase in grain boundary energy that is caused by an increase in the boundary area during the formation of a recrystallized grain [73]:

$$f^{(i,j)} = e_{dst}^{(i,j)} - e_{gb}^{(i,j)} \Delta s / \Delta v \geq 0, \quad (15)$$

where Δs is the increase in the boundary area when a subgrain volume (a DRX nucleus) changes by Δv , $e_{dst}^{(i,j)}$ is the difference between the specific energies of adjacent subgrains stored per unit volume i and j , and $e_{gb}^{(i,j)}$ is the energy per area unit for the boundary between the i -th and j -th subgrains.

In order to apply criterion (15) and calculate the values of Δs , Δv , we introduce an additional mesolevel-II variable (a characteristic subgrain size) r . We speak of nuclei that are spherical in shape and assume that the initial subgrain size distribution obeys the Rayleigh law [62,63]. If the necessary experimental data are available, then we can use other distribution laws. It is assumed that the size of subgrains does not change during deformation. The recrystallization nuclei are located near the boundary (a set of facets). Each facet of the grain under consideration is assigned a sample of subgrain sizes (recrystallization nuclei) r according to the Rayleigh law. The validity of the recrystallization criterion (15) is verified for every subgrain separated by the high-angle boundary from the neighboring ones.

We do not consider here the mechanism governing the formation of new grains from subgrains during their rotation until the high-angle misorientations with the parent grain occur. We suppose that new grains are formed only during the DRX process. In the volume of one grain, the subgrains are separated by the low-angle boundaries and are slightly misoriented relative to each other. Thus, it is reasonable to believe that the stored energy e_{st} , determined by relation (15), is approximately the same in all subgrains within one grain. The data on the stored energy e_{st}^I calculated at mesolevel-I and needed to verify the validity of the recrystallization criterion (15) are transmitted to mesolevel-II. Thus, we have:

$$e_{st}^{II} = e_{st}^I \stackrel{def}{=} e_{st}, \quad (16)$$

where e_{st}^{II} is the stored energy at mesolevel-II. The difference in stored energy between the subgrains belonging to different grains but having a common high-angle boundary may be significant.

In fulfilling criterion (15), we assume that DRX nuclei are active and that they are separated into individual grains. This separation proceeds in two stages. At the first stage, when condition (15) is satisfied, the active nuclei are added to the static model; at the second stage, the polyhedral grain structure is rearranged by considering new recrystallized grains. The description of this method is given in Section 3. The new DRX grains are considered to be low-defective; thus, all internal variables of a recrystallized grain in the annealed material correspond to the reference configuration, with the exception of the new grain orientation determined by the tensor \mathbf{o} and the geometric characteristics. A refined definition of these characteristics is also given in Section 3. The volume of the new DRX grain is subtracted from the volume of the parent grain. Experimental data [5,61] indicated that for the mechanism of DRX nuclei formation considered here, the new (recrystallized) grains have a consistent orientation coherency with the parent grain. It was shown that the new grain is separated from the parent grain by a high angle boundary, and it has initial orientation with respect to the parent grain within the range from 10 to 15° with a random axis of rotation [5,61]. The DRX grain orientation with respect to the neighboring

(absorbed) grain is arbitrary (Figure 1b). At this stage of modeling, in order to evaluate the influence of grain boundary hardening, we assume that the new grain is surrounded by six identical facets, and the neighboring grains are determined in a random way.

The migration of the high-angle boundary of a new grain occurs at temperatures sufficient to ensure its mobility. The Arrhenius law is used to study the effect of temperature on the high-angle mobility [5]:

$$m = m_0 \exp\left(-\frac{Q}{R\theta}\right), \quad (17)$$

where θ is the absolute temperature; R is the universal gas constant; Q is the activation energy of the grain boundary migration; m_0 is the experimentally determined pre-exponent. The high angle boundary migration velocity v_m is determined by the product of the driving force f (the indexes denoting the neighboring crystallites are omitted) and the mobility m [5]:

$$v_m = fm. \quad (18)$$

At this stage of model development, we assume for simplicity that the shape of the recrystallization nuclei is spherical (the refine geometry of recrystallized grains is described in Section 3) and that each new recrystallized grain penetrates deep into the neighboring grain. In this case, v_m is equal to the rate of change of the ball radius r , which describes the shape of the recrystallized grain, i.e., $\dot{r} = v_m$ (the dot above r shows the material derivative). The absorbed grain volume is reduced by the volume of recrystallized grains. The volume fraction of the recrystallized material X in a polycrystal is determined through the following relation:

$$X = \frac{V_r}{V_0}, V_r = \sum_{i=1}^{N_r} v_r^{(i)}, \quad (19)$$

where V_0 is the initial value of the representative volume of a polycrystal under consideration; V_r is the DRX material volume; N_r is the number of DRX grains; $v_r^{(i)} = \frac{4}{3}\pi r^{(i)3}$ is the i -th DRX grain volume.

3. Rearrangement of the Grain Structure Formed during High-Temperature Deformation with Recrystallization

During recrystallization, the grain structure varies continuously; changes are related to changes in the number, shape, and size of the grains under study. We propose a method for the formation of the grain structure and its rearrangement during deformation, which allows consideration of the formation of new DRX grains. The developed method is applied for a statistical model, one of the main tasks of which is to solve the problem of grain structure rearrangement during recrystallization and to establish a correspondence between the geometric image of a real grain structure described by polyhedra (Figure 3a) and its model representation in the framework of the modified statistical model (Figure 3b). In this model, the grain structure is determined by such internal variables as the grain volume v_g , the facets with the normal \mathbf{n}_i and the area s_j (where j denotes the number of a facet), and through assigning neighboring grains to the considered grain. First, the initial polyhedral grain structure is formed in the software package Neper [59]. Then, the obtained data are transferred to the calculation module of the statistical model for the implementation of the inelastic deformation model described above.

The modeling of active recrystallization nuclei proceeds in two stages. Information on the first stage of the simplified description is given in the previous section of this article. During this stage, subgrains (DRX nuclei) are assigned to each facet of the initial grains. As the recrystallization criterion (15) is met, these subgrains are considered as independent grains added, without taking into account their geometric shape, to sample data of the statistical model. When the volume fraction of active recrystallization nuclei f_{cr} reaches its critical value of 20% (found in computational experiments), the second stage at which the new grains are introduced into the geometric model of a representative volume begins. To

this end, we again start the procedure for generating a polyhedral grain structure in the Neper program [59]. This allows us to take into account new grains and to find whether the statistical model is consistent with the calculation scheme. With the software package Neper, we construct a polyhedral structure on the basis of the laws of distribution through the sphericity parameters ψ_g (the ratio of the surface area of the sphere, whose volume is equal to the volume of a considered grain to the grain surface area) and the normalized grain size d_{eq} ($d_{eq} = \frac{d}{\langle d \rangle}$, where d is the grain size defined as the radius of a sphere of equivalent volume and $\langle d \rangle$ is the average grain size). To this end, the Neper involves the numerical implementation of optimization methods [59].

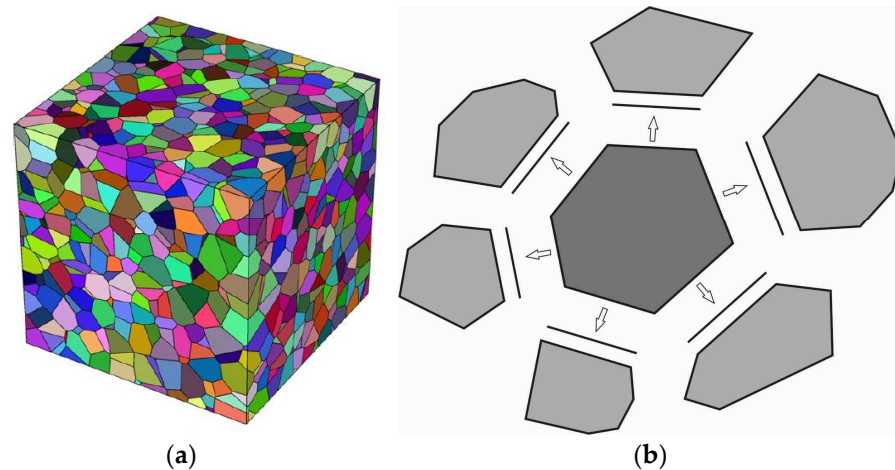


Figure 3. Polyhedral representation of polycrystal grains (a) and scheme of the grain structure in the statistical model (b).

After the polyhedral grain structure is formed in Neper, the obtained data (grain volumes, normals, and facet areas with indication of neighboring grains) are transferred to the statistical model, where the grain structure is redefined. Note that new crystallites are introduced into the geometric structure of the considered region through DRX simulations; previously, the statistical model does not take into account the geometry of this region. To compare the initial and newly deformed structures, we consider two types of grains: original defective grains and new DRX grains. The main geometric characteristic of grains is their size, which is determined by the volume of an equivalent sphere. The defect structure is primarily characterized by the stored energy e_{st} . At critical deformation ϵ_c , large non-recrystallized grains usually coexist with fine recrystallized grains (Figure 1b), and a bimodal grain size distribution is generally observed. In this case, we distinguish a cluster of grains, namely a large “consumed” defective grain surrounded by fine DRX grains for the initial grain structure (Figure 4). Initially, we compare all grains according to their characteristic sizes. For this purpose, the square of difference in grain sizes is assumed to be minimal for original and new grain structures. At later recrystallization stages where the grain size distribution is close to unimodal (Figure 1d), the grains are also compared vs. their sizes. In both cases, the variant of the grain structure, determined with regard to the best fit of grain sizes, is taken as the initial approximation. Then, the genetic algorithm method [74] is applied to perform a purposeful selection of grains. This allows us to reach a minimum in distribution of the difference between the energies stored in the grains of original and new structures (comparison is made by the mathematical expectation of the stored energy distribution and grain sizes). The conditions for the migration of grain boundaries before and after the geometric structure rearrangement will be statistically equivalent, which ensures “continuity” in the simulation of the recrystallization process.

Next, we describe the grain structure evolution in terms of a statistical model. The grain structure is subjected to thermomechanical loading change for the following two reasons. The first is due to mechanical influences, mainly due to the movement of dislocations

during inelastic deformation, whereby the areas and normals of grain facets vary according to the known formulas of continuum mechanics [75]:

$$\hat{s}_i = s_i \det(\mathbf{f}) \left(\mathbf{n}_i \cdot \mathbf{f}^{-1} \cdot \mathbf{f}^{-T} \cdot \mathbf{n}_i \right)^{-1/2}, \hat{\mathbf{n}}_i = \left(\mathbf{n}_i \cdot \mathbf{f}^{-1} \cdot \mathbf{f}^{-T} \cdot \mathbf{n}_i \right)^{-1/2} \mathbf{f}^T \cdot \mathbf{n}_i \quad (20)$$

where s_i, \hat{s}_i are the areas of facets in the reference and actual configurations with corresponding normal $\mathbf{n}_i, \hat{\mathbf{n}}_i$; $\det(\cdot)$ is the operation of a determinant; i is the facet number. The changes in grain volume observed during elastoviscoplastic deformation are neglected. The statistical model of inelasticity is based on the Voigt hypothesis, and a deformation gradient \mathbf{f} is known at every instant of deformation.

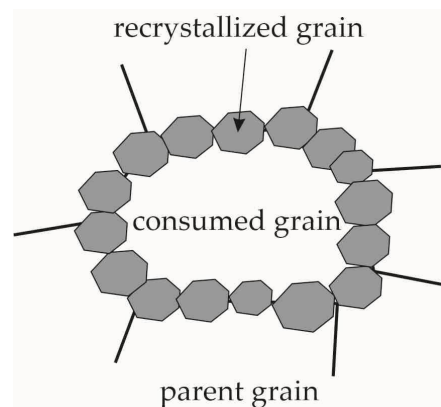


Figure 4. Scheme used for modeling a cluster of grains (a “consumed” defective grain surrounded by DRX grains).

The second mechanism governing the grain structure changes is diffusion, which is realized when the high-angle boundaries migrate deep into the defective grains in the direction of the outer normal. Due to this process, both the numbers of grains and their neighbors (adjacent grains) change, and hence there arises a need for reconstructing a polyhedral grain structure in the software package Neper. In DRX simulation, the known value is the boundary migration velocity v_m , which is determined by Equation (18) for each facet at every instant of thermomechanical process. The driving force f is determined by relation (15), where $\Delta s, \Delta v$ mean that the area and volume, respectively, of recrystallized grains increase. As the grain grows, the second term in (15) does not contribute to f , meaning this value is almost completely determined by the difference in stored energy between neighboring grains. It is assumed that the migration velocity of the boundary facet is directed along the outer normal $\hat{\mathbf{n}}$ of the boundary facet, i.e., the following ratio is true:

$$\mathbf{v}_m = v_m \hat{\mathbf{n}}. \quad (21)$$

Due to its significant non-linearity, the problem is solved by a step-by-step method, where the step size Δt is determined from the analysis of the results of a series of numerical experiments. It is assumed that in the time interval Δt , v_m is constant. The velocity vector \mathbf{u}_m resulting from the boundary migration is calculated for Δt by integrating (21) as:

$$\mathbf{u}_m = \int_{\tau}^{\tau+\Delta t} v_m \hat{\mathbf{n}} dt = v_m \hat{\mathbf{n}} \Delta t. \quad (22)$$

Figure 5 presents a scheme illustrating how the grain shape changes during the migration of the facet with the normal $\hat{\mathbf{n}}$. Further, we will consider only the migrating facet and the adjacent facets. The elements of the migrating facet are denoted by the index m and the adjacent facets by the index f . In this model, the grain structure is represented by flat sections, meaning the “bending” of the boundary cannot be described. However, there

is a possibility of considering the rotation of the adjacent facets under the assumption that an increase in volume is provoked by this effect (see Figure 5). In this case, it is assumed that the polyhedron remains convex. In the statistical model, the change in the geometry of the polyhedra is not actually simulated. The characteristic size and sphericity of grains needed for rearrangement of the polyhedral grain structure in Neper are determined in a simplified way after a certain number of time steps.

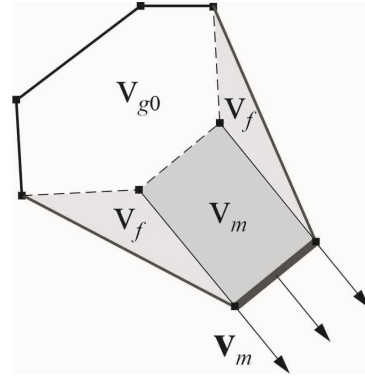


Figure 5. Scheme of facet migration.

According to the scheme given in Figure 5, the volume of the recrystallized part of the grain occurred due to the facet migration v_r is calculated as the sum of two terms:

$$v_r = v_m + v_{\Sigma f} = \beta v_m, \quad (23)$$

where v_m is the volume swept by the mobile facet; $v_{\Sigma f}$ is the total volume made up of the “rotation” of the facets; $\beta > 1$ is the parameter describing the change in the volume of a DRX grain due to the migration of the facets. The relation for v_m is determined assuming that the swept volume is the volume of a rectangular parallelepiped:

$$v_m = u_m s_m, \quad (24)$$

where s_m is the area of the migrating facet. During the facet migration and assuming that the rectangular shape of the facets remains unchanged, the area of each of the adjacent facets increases by the value s_r :

$$s_r = u_m \sqrt{s_f}, \quad (25)$$

where s_f is the initial area of the facet adjacent to the migrating facet. For the consumed grain adjacent to the migrating facet, the volume decreases by the value v_r calculated by relation (23), and the areas of the neighboring grain facets adjacent to the migrating facet decrease by the values determined by (25). If the volume of the neighboring grain reduces to zero (to an accuracy of computational error), then it is replaced by the grain from a representative volume of the statistical model. This grain is determined from the facet of the closest orientation, which is assumed to be conjugated with the migrating facet.

Finally, the characteristic size r_g (to do this, the sphere of equal volume is associated with a grain) and sphericity ψ_g are obtained for each grain:

$$r_g = \left(\frac{3}{4\pi} v_g \right)^{1/3}, \quad \psi_g = \frac{4\pi r_g^2}{s_g}, \quad (26)$$

where $v_g = v_{g0} + v_r$, $s_g = s_{g0} + s_r$ is the volume and area of the grain determined by the above-mentioned relations. The distributions of r_g and ψ_g obtained for the considered representative volume are transferred to Neper to construct a new polyhedral structure, and then the grain structure data are introduced into the statistical model; this procedure is repeated many times.

4. Simulation Results and Their Analysis

This paper investigates the inelastic deformation of a copper polycrystal sample. The multilevel model parameters are given in Table 1.

Table 1. The parameters of the multilevel model of inelastic deformation.

Parameter	Value	Literature Source
Π_{1111}	140 GPa	[76]
Π_{1122}	104 GPa	[76]
Π_{1313}	63 GPa	[76]
G	39 GPa	[77]
τ_{c0}	10 MPa	Identification procedure
τ_{sat}	27 MPa	Identification procedure
h_0	200 MPa	Identification procedure
a	1.4	Identification procedure
q_{lat}	1.4	[72]
$\dot{\gamma}_0$	0.001 s^{-1}	[72]
m	83	[72]
η	1.0	Identification procedure
α	0.0012	Identification procedure
e_{gb}	0.625 J/m^2	[5]
r_0	$0.25 \text{ }\mu\text{m}$	[62]
Q	121 kJ/mol	[5]
m_0	$1.5 \times 10^{-6} \text{ s}\cdot\text{m}^2/\text{kg}$	[5]

The identification of material parameters for the inelastic deformation model (Table 1) was carried out on the basis of the experimental data [78]. This table includes the results of experimental studies of the stress–strain state of cylindrical samples measuring 8 mm in diameter and 12 mm in height. The uniaxial compression tests were carried out at a temperature of 775 K and at a strain rate of $2 \times 10^{-3} \text{ s}^{-1}$ for a polycrystal of commercial pure copper, which was pre-treated by annealing at 973 K for two hours [78]. The values of the anisotropic elastic moduli of the grain Π_{ijkl} [76] and the shear modulus of the polycrystal G [77] correspond to the absolute temperature 775 K adopted for the numerical experiment. In order to perform specific calculations by applying an advanced statistical model, the grain structure of a polycrystal should be given in the reference configuration (the procedure for grain structure formation is described in [79]). Based on the available experimental data, statistic laws were derived for the distribution of normalized grain size d_{eq} and sphericity ψ_g of the copper polycrystal grains. The average polycrystalline copper grain size d_0 was $78 \text{ }\mu\text{m}$ [78]. To approximate the grain size distribution, the lognormal law was used [80,81]. According to the data collected from the microsectional analysis [78], there is a scattering in grain sizes, which is characteristic of annealed materials. The following parameters are needed to specify a log-normal distribution: $\mu = 3.86$, $\sigma = 1$ such that the mathematical expectation $\exp(\mu + \sigma^2/2)$ be equal to the average grain size $d_0 = 78 \text{ }\mu\text{m}$. If the representative experimental data on grain size distribution exist, then there is no difficulty in solving the optimization problem of determining the statistical distribution law and identifying its parameters, as was done in [82] for subgrain size distributions. We suppose that in the initial state, the copper sample after annealing has predominantly equiaxed grains with an average sphericity $\langle \psi_g \rangle = 0.90$; the data on sphericity are given in [83]. Figure 6 presents the grain size distribution d_{eq} and grain sphericity ψ_g histograms obtained based on existing experimental data [78,83].

The applied statistical two-level mathematical model is based on Voigt's hypothesis. The kinematic influence is prescribed and the velocity gradient is known. Plastic deformations corresponding to uniaxial deformation are considered [6]:

$$\hat{\nabla} \mathbf{V} = \dot{\gamma} \mathbf{k}_{01} \mathbf{k}_{01} - \frac{\dot{\gamma}}{2} \mathbf{k}_{02} \mathbf{k}_{02} - \frac{\dot{\gamma}}{2} \mathbf{k}_{03} \mathbf{k}_{03}, \quad (27)$$

where $\mathbf{k}_{0i} = \mathbf{k}_0^i$ is the orthonormal basis of the laboratory coordinate system; $\dot{\gamma}$ is the prescribed deformation velocity.

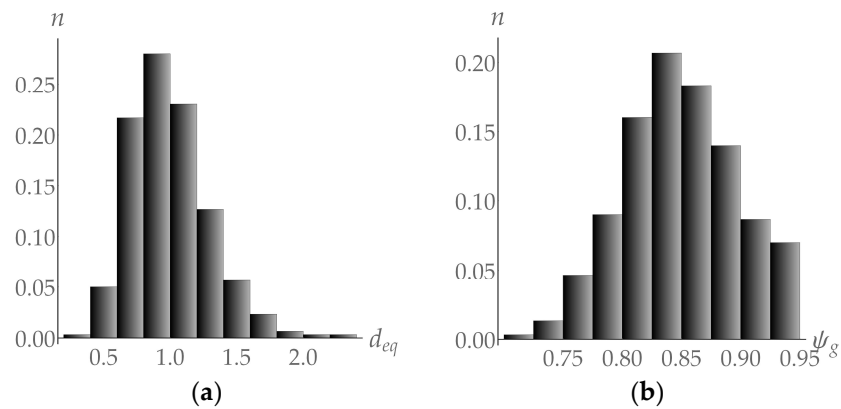


Figure 6. Normalized grain size distribution d_{eq} (non-dimensional) (a) and grain sphericity ψ_g (non-dimensional) (b) histograms.

Further, we present the results of the computational experiments carried out at deformation velocity $\dot{\gamma} = 10^{-3} \text{ s}^{-1}$ and temperature $\theta = 775 \text{ K}$. The loading diagram (with and without the recrystallization process) is given in Figure 7a, and the corresponding deformation textures formed after the end of plastic deformation are shown in Figure 7b. We emphasize a significant contribution of recrystallization to the deformation texture “blurring”, which is attributed to the appearance of new DRX grains with an orientation consistent with the parent grain—numerous points for DRX grains are seen on the pole figure near the point reflecting the orientation of the parent grain.

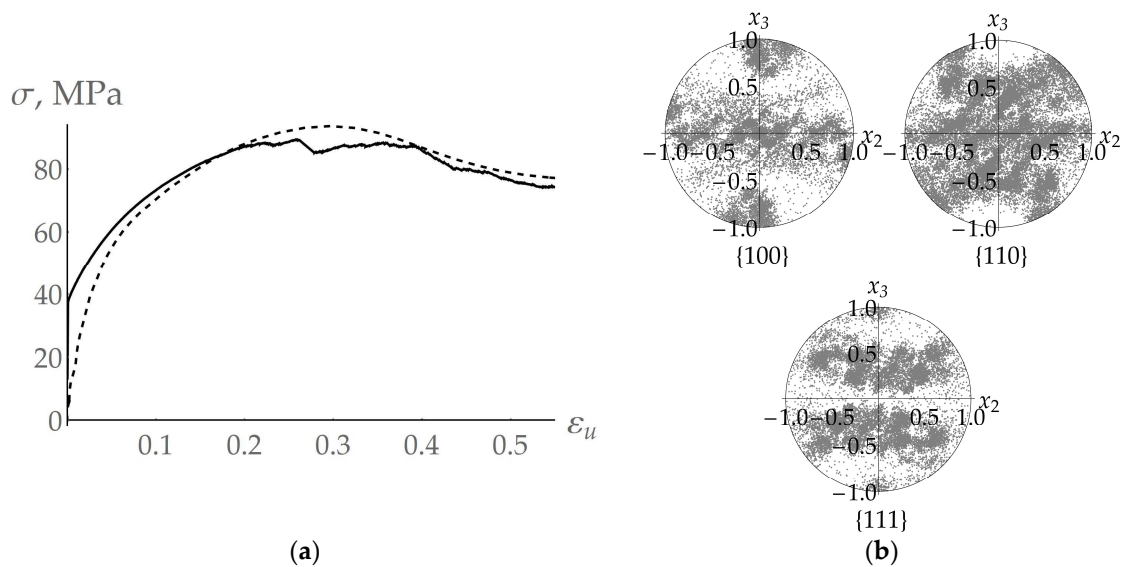


Figure 7. Loading diagram for the copper polycrystal at deformation velocity $\dot{\gamma} = 10^{-3} \text{ s}^{-1}$ and temperature $\theta = 775 \text{ K}$ (dashed curve—experiment [78], solid curve—calculations) (a). Calculated pole figures {100}, {110}, and {111} at the end of deformation (b).

Figure 8a illustrates the evolution of the average grain size $\langle r_g \rangle$ during plastic deformation. Figure 8b shows a change in the average value of the facet area $\langle s_g \rangle$. Figure 8c demonstrates the evolution of the ratio of the average grain volume to the facet area $\phi_g = \langle s_g \rangle / \langle v_g \rangle$. Notice that the recrystallization process refines the initially coarse polycrystal grains. At the end of deformation, the average grain size reaches a value of $14 \mu\text{m}$. The fraction of high-angle boundaries also increases due to the appearance of many recrystallized grains (Figure 8c). Initially, the representative volume of the polycrystal contains

300 grains, and at the end of deformation it consists of 2017 grains. In the reference configuration, the edge of the representative volume in the form of a cube is about 421 μm . At the end of deformation, the size of the edge along which tension occurred is 767 μm , and the remaining two edges are 312 μm in size. The violations of the curves correspond to the instants of time at which the polyhedral grain structure rearranges in Neper.

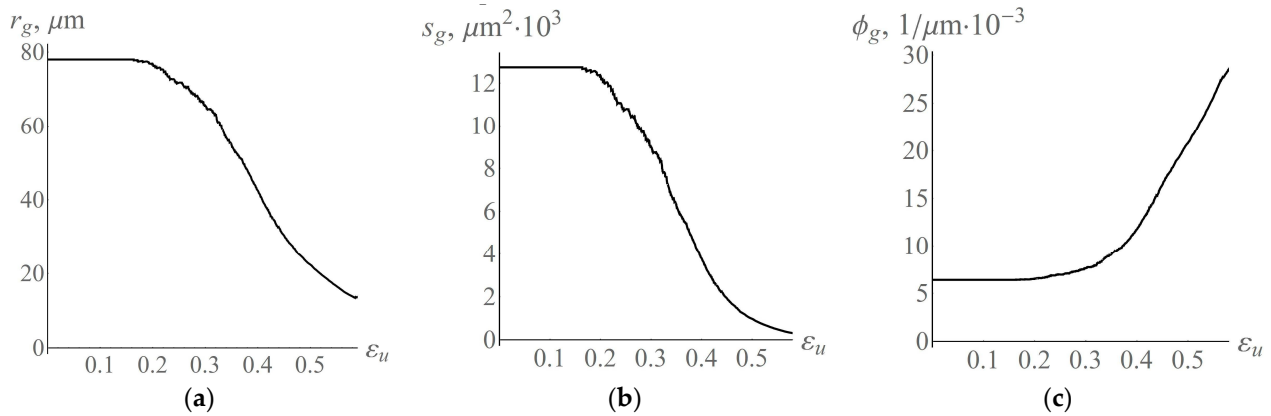


Figure 8. Evolution of average grain size (a) and average grain facet area (b) and the ratio of the average grain volume to the facet area (c) during plastic deformation.

Figure 9 presents the polyhedral structures formed in Neper. These structures correspond to the instant of deformation $\epsilon_m = 0.25$ at which the stress tensor σ_m reaches its maximum (Figure 9a) and to the end of deformation $\epsilon_f = 0.53$ (Figure 9b). It is interesting that at the instant of deformation ϵ_m , both large initial grains and new grains with a small size appear. At the instant of deformation ϵ_f , practically no large grains are kept.

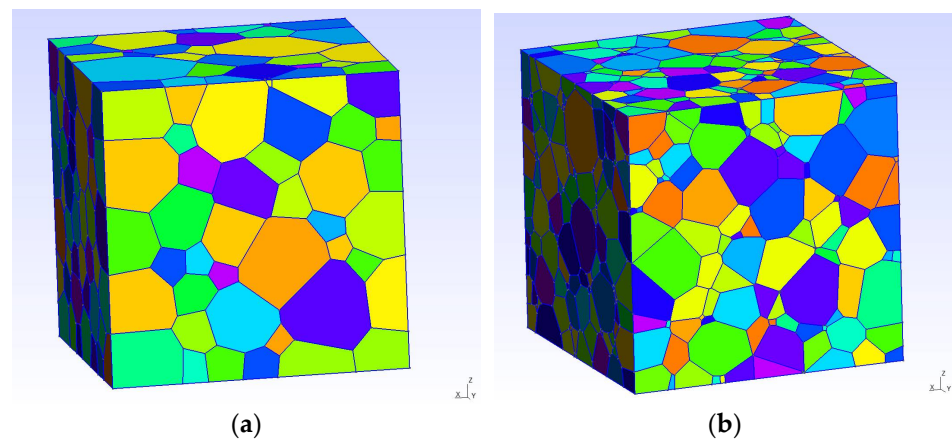


Figure 9. Polyhedral grain structure obtained using Neper at the instants of deformation ϵ_m (a) and ϵ_f (b).

This is confirmed by the grain size distribution r_g (Figure 10a,b) and sphericity ψ_g (Figure 10c,d) histograms, plotted for two different instants of deformation ϵ_m, ϵ_f . For ϵ_m , the distribution of grain sizes r_g and sphericity ψ_g is a bimodal distribution with two characteristic peaks that reflect the initial stage of DRX implementation. At the end of deformation ϵ_f , the structure becomes fine-grained (Figure 10b) and equiaxed (Figure 10d) with an average grain size of about 14 μm . The grain size distribution (Figure 10b) is characterized by the presence of a fraction (about 9%) of non-recrystallized grains with sizes that range from 30 μm to 150 μm . The sizes of non-recrystallized grains significantly exceed those of recrystallized grains, as evidenced by the data from Figure 10a,b. The level of energy stored on defects in non-recrystallized grains is much higher as compared to recrystallized grains. Therefore, the current critical stresses caused by the interaction of mobile dislocations with forest dislocations (relation (8)) exhibit high values. On the other

hand, in large non-recrystallized grains, the contribution of the grain size to strengthening due to the interaction of mobile dislocations with grain boundaries is smaller (relation (9)). During the recrystallization process, large initial grains are gradually replaced by less defective recrystallized grains of a smaller size, which causes the current critical stress values to reduce. Due to the competing processes of hardening and softening, the resistance to deformation becomes stationary. The original non-recrystallized grain boundaries are non-equilibrium (new recrystallized grains are formed on these boundaries), which promotes the subsequent absorption of non-recrystallized grains. Under further deformation and at increasing stored energy level in recrystallized grains, these grains may become absorbed because of the appearance of less defective grains, which is an indication of the cyclic nature of the process of intermittent dynamic recrystallization. Thus, the amount of recrystallized material should be determined for each cycle separately.

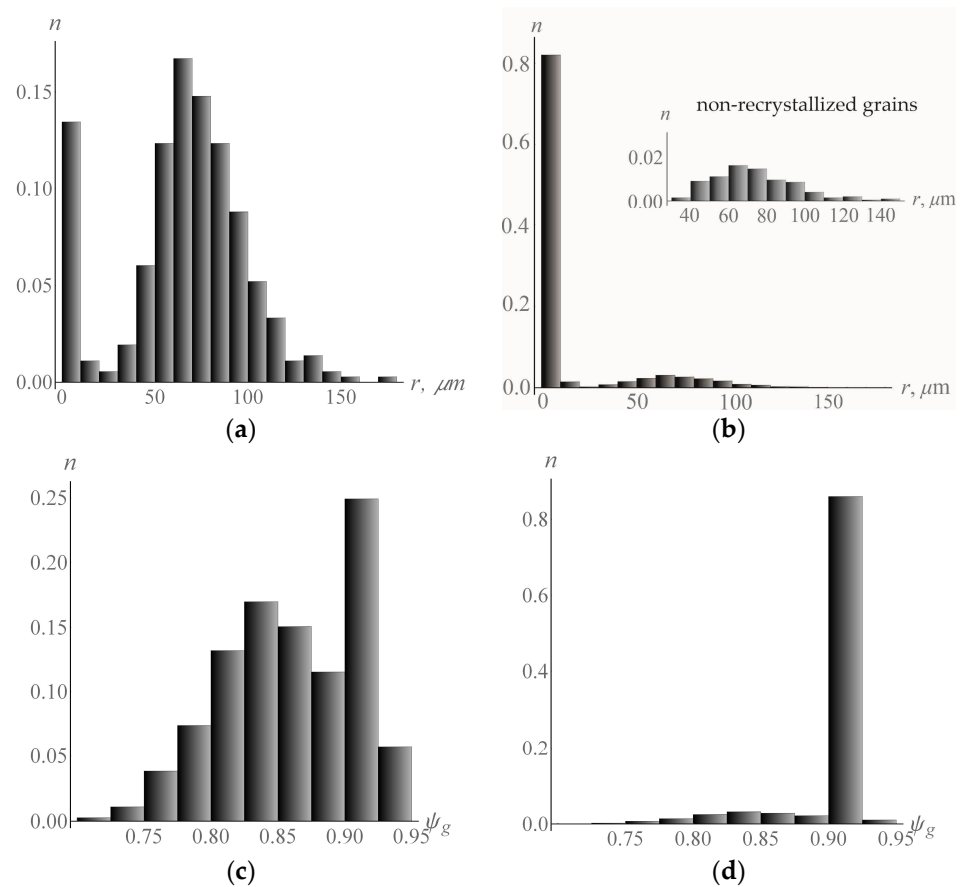


Figure 10. Grain size distribution r_g (a,b) and grain sphericity ψ_g (c,d) histograms at different instants of deformation ε_m and ε_f , respectively.

5. Discussion and Conclusions

The construction of models that are suitable for designing functional materials is a complex task that requires a careful study of many aspects of their behavior. The polycrystalline materials used in industry for the manufacture of real products are alloys. As a rule, these materials must meet the yield stress and strength requirements, meaning they are difficult to deform and their processing takes place at elevated deformation temperatures. During material processing, processes accompanying this deformation occur, among which the most significant with regard to the material structure evolution is recrystallization. This is why the description of recrystallization should be included in the models under study. In contrast to pure metals, recrystallization that develops in alloys depends on the behavior of impurity atoms and particles of secondary phases, which have a retarding effect on the motion of recrystallized grain boundaries. Moreover, the particles of sec-

ondary phases are also the sites for the predominant formation of recrystallization nuclei. The above-mentioned structural metals exhibit the ability to undergo solid-state phase transformations, meaning they have two or more phases in original billets, or experience solid-state phase transformations during thermomechanical processing. The occurrence of different phases and the increasing complexity of the model parameter identification process raise the non-trivial question of modeling the interaction between them. Hence, it follows that the development of a universal model capable of describing a variety of processes that occur during the thermomechanical processing of real materials is a challenging but feasible task. By analyzing the obtained results, we can conclude that the multilevel modeling approach based on the introduction of internal variables offers the possibility of developing additional blocks of a mathematical constitutive model needed to describe different physical mechanisms observed during thermo-mechanical treatment and for their further integration into in the full model to describe metal processing. The statistical model proposed in this work was primarily used to study the grain structure evolution in a copper polycrystal during its recrystallization and the coupled response of the stress–strain state of a half-crystal representative volume. Furthermore, this model has potential for determining thermomechanical factors that govern the formation of the necessary (given by statistical laws) grain structure, which ensures the required material properties.

We modified the advanced statistical model of inelastic deformation with the intent of introducing a process of dynamic recrystallization. For this purpose, we developed a method for describing the grain structure evolution in the framework of a geometrical approach based on Laguerre polyhedra. The obtained data were analyzed and transferred to the modified statistical model. The developed model has a number of advantages compared to existing models, namely it has higher computational efficiency and is able to take into account the physical interactions between neighboring grains. The results of the computational experiments obtained with this model are in good agreement with the experimental data. The model makes it possible to evaluate the effects associated with the refinement of the grain structure and its transformation to an equiaxed shape and to analyze the tendency of the average grain size to decrease. We also proposed a method to introduce a description of new recrystallized grains into the model and a method to establish a correspondence between the geometric image of a real grain structure, described by a polyhedral, and the grain structure of a statistical model, determined by a set of volumes, normals, and grain facet areas, indicating the neighboring grains in the recrystallization process.

Author Contributions: Conceptualization, P.T. and N.K.; methodology, P.T. and N.K.; software, A.P.; validation, A.P., N.K. and P.T.; formal analysis, N.K. and A.P.; investigation, N.K., P.T. and A.P.; data curation, N.K. and A.P.; writing—original draft preparation, N.K.; writing—review and editing, P.T., N.K. and A.P.; visualization, N.K. and A.P.; supervision, P.T.; funding acquisition, N.K. All authors have read and agreed to the published version of the manuscript.

Funding: The study was carried out with a financial support from the Ministry of Education and Science of the Russian Federation as part of the implementation of the national project “Science and Universities” (the state task fulfillment in the laboratory of multilevel structural and functional materials modeling, project no. FSNM-2021-0012).

Conflicts of Interest: The authors declare no conflict of interest.

References

1. Hsu, E.; Carsley, J.E.; Verma, R. Development of Forming Limit Diagrams of Aluminum and Magnesium Sheet Alloys at Elevated Temperatures. *J. Mater. Eng. Perform.* **2008**, *17*, 288–296. [[CrossRef](#)]
2. Zhang, R.; Shao, Z.; Lin, J. A Review on Modelling Techniques for Formability Prediction of Sheet Metal Forming. *Int. J. Lightweight Mater. Manuf.* **2018**, *1*, 115–125. [[CrossRef](#)]
3. Zheng, G.; Pang, T.; Sun, G.; Wu, S.; Li, Q. Theoretical, Numerical, and Experimental Study on Laterally Variable Thickness (LVT) Multi-Cell Tubes for Crashworthiness. *Int. J. Mech. Sci.* **2016**, *118*, 283–297. [[CrossRef](#)]
4. Sun, G.; Zhang, H.; Wang, R.; Lv, X.; Li, Q. Multiobjective Reliability-Based Optimization for Crashworthy Structures Coupled with Metal Forming Process. *Struct. Multidisc. Optim.* **2017**, *56*, 1571–1587. [[CrossRef](#)]

5. Humphreys, F.J.; Hatherly, M. *Recrystallization and Related Annealing Phenomena*; Elsevier: Amsterdam, The Netherlands, 2012; ISBN 978-0-08-098388-2.
6. Trusov, P.V.; Shveykin, A.I. *Multilevel Models of Mono- and Polycrystalline Materials: Theory, Algorithms, Application Examples*; SB RAS: Novosibirsk, Russia, 2019. (In Russian)
7. Montheillet, F. Moving Grain Boundaries During Hot Deformation of Metals: Dynamic Recrystallization. In *Moving Interfaces in Crystalline Solids*; Fischer, F.D., Ed.; CISM International Centre for Mechanical Sciences; Springer: Vienna, Austria, 2005; pp. 203–256. ISBN 978-3-211-27404-0.
8. Zhou, G.; Li, Z.; Li, D.; Peng, Y.; Zurob, H.S.; Wu, P. A Polycrystal Plasticity Based Discontinuous Dynamic Recrystallization Simulation Method and Its Application to Copper. *Int. J. Plast.* **2017**, *91*, 48–76. [[CrossRef](#)]
9. Chen, S.F.; Li, D.Y.; Zhang, S.H.; Han, H.N.; Lee, H.W.; Lee, M.G. Modelling Continuous Dynamic Recrystallization of Aluminum Alloys Based on the Polycrystal Plasticity Approach. *Int. J. Plast.* **2020**, *131*, 102710. [[CrossRef](#)]
10. Liu, F.; Fa, T.; Chen, P.H.; Wang, J.T. Steady-State Characteristics of Fcc Pure Metals Processed by Severe Plastic Deformation: Experiments and Modelling. *Philos. Mag.* **2020**, *100*, 62–83. [[CrossRef](#)]
11. Hansen, N. Cold Deformation Microstructures. *Mater. Sci. Technol.* **1990**, *6*, 1039–1047. [[CrossRef](#)]
12. Asaro, R.J. Micromechanics of Crystals and Polycrystals. *Adv. Appl. Mech.* **1983**, *23*, 1–115. [[CrossRef](#)]
13. Roters, F.; Eisenlohr, P.; Hantcherli, L.; Tjahjanto, D.D.; Bieler, T.R.; Raabe, D. Overview of Constitutive Laws, Kinematics, Homogenization and Multiscale Methods in Crystal Plasticity Finite-Element Modeling: Theory, Experiments, Applications. *Acta Mater.* **2010**, *58*, 1152–1211. [[CrossRef](#)]
14. McDowell, D.L. A Perspective on Trends in Multiscale Plasticity. *Int. J. Plast.* **2010**, *9*, 1280–1309. [[CrossRef](#)]
15. Acar, P.; Ramazani, A.; Sundararaghavan, V. Crystal Plasticity Modeling and Experimental Validation with an Orientation Distribution Function for Ti-7Al Alloy. *Metals* **2017**, *7*, 459. [[CrossRef](#)]
16. Galán-López, J.; Hidalgo, J. Use of the Correlation between Grain Size and Crystallographic Orientation in Crystal Plasticity Simulations: Application to AISI 420 Stainless Steel. *Crystals* **2020**, *10*, 819. [[CrossRef](#)]
17. Taylor, G.I. Plastic Strain in Metals. *J. Inst. Met.* **1938**, *62*, 307–324.
18. Kocks, F.; Mecking, H. Physics and Phenomenology of Strain Hardening: The FCC Case. *Prog. Mater. Sci.* **2003**, *48*, 171–273. [[CrossRef](#)]
19. Zhang, K.; Holmedal, B.; Hopperstad, O.S.; Dumoulin, S.; Gawad, J.; Van Bael, A.; Van Houtte, P. Multi-Level Modelling of Mechanical Anisotropy of Commercial Pure Aluminium Plate: Crystal Plasticity Models, Advanced Yield Functions and Parameter Identification. *Int. J. Plast.* **2015**, *66*, 3–30. [[CrossRef](#)]
20. Lebensohn, R.A.; Liu, Y.; Ponte Castañeda, P. On the Accuracy of the Self-Consistent Approximation for Polycrystals: Comparison with Full-Field Numerical Simulations. *Acta Mater.* **2004**, *52*, 5347–5361. [[CrossRef](#)]
21. Lebensohn, R.A.; Tomé, C.N.; Castañeda, P.P. Self-Consistent Modelling of the Mechanical Behaviour of Viscoplastic Polycrystals Incorporating Intragranular Field Fluctuations. *Philos. Mag.* **2007**, *87*, 4287–4322. [[CrossRef](#)]
22. Beyerlein, I.J.; Knezevic, M. Review of Microstructure and Micromechanism-Based Constitutive Modeling of Polycrystals with a Low-Symmetry Crystal Structure. *J. Mater. Res.* **2018**, *33*, 3711–3738. [[CrossRef](#)]
23. Yaghoobi, M.; Ganesan, S.; Sundar, S.; Lakshmanan, A.; Rudraraju, S.; Allison, J.E.; Sundararaghavan, V. PRISMS-Plasticity: An Open-Source Crystal Plasticity Finite Element Software. *Comput. Mater. Sci.* **2019**, *169*, 109078. [[CrossRef](#)]
24. Feather, W.G.; Lim, H.; Knezevic, M. A Numerical Study into Element Type and Mesh Resolution for Crystal Plasticity Finite Element Modeling of Explicit Grain Structures. *Comput. Mech.* **2021**, *67*, 33–55. [[CrossRef](#)]
25. Trusov, P.V.; Kondratev, N.S.; Yanz, A.Y. A Model for Static Recrystallization through Strain-Induced Boundary Migration. *Phys. Mesomech.* **2020**, *23*, 97–108. [[CrossRef](#)]
26. Shveykin, A.; Trusov, P.; Sharifullina, E. Statistical Crystal Plasticity Model Advanced for Grain Boundary Sliding Description. *Crystals* **2020**, *10*, 822. [[CrossRef](#)]
27. Trusov, P.V.; Shveykin, A.I. Multilevel Crystal Plasticity Models of Single- and Polycrystals. Statistical Models. *Phys. Mesomech.* **2013**, *16*, 23–33. [[CrossRef](#)]
28. Trusov, P.V.; Shveykin, A.I. Multilevel Crystal Plasticity Models of Single- and Polycrystals. Direct Models. *Phys. Mesomech.* **2013**, *16*, 99–124. [[CrossRef](#)]
29. Rollett, A.D. Overview of Modeling and Simulation of Recrystallization. *Prog. Mater. Sci.* **1997**, *42*, 79–99. [[CrossRef](#)]
30. Huang, K.; Logé, R.E. A Review of Dynamic Recrystallization Phenomena in Metallic Materials. *Mater. Des.* **2016**, *111*, 548–574. [[CrossRef](#)]
31. Tan, K.; Li, J.; Guan, Z.; Yang, J.; Shu, J. The Identification of Dynamic Recrystallization and Constitutive Modeling during Hot Deformation of Ti55511 Titanium Alloy. *Mater. Des.* **2015**, *84*, 204–211. [[CrossRef](#)]
32. Irani, M.; Joun, M. Determination of JMAK Dynamic Recrystallization Parameters through FEM Optimization Techniques. *Comput. Mater. Sci.* **2018**, *142*, 178–184. [[CrossRef](#)]
33. Puchi-Cabrera, E.S.; Guérin, J.D.; La Barbera-Sosa, J.G.; Dubar, M.; Dubar, L. Plausible Extension of Anand’s Model to Metals Exhibiting Dynamic Recrystallization and Its Experimental Validation. *Int. J. Plast.* **2018**, *108*, 70–87. [[CrossRef](#)]
34. Vandermeer, R.A.; Rath, B.B. Microstructural Modeling of Recrystallization in Deformed Iron Single Crystals. *Metall. Mater. Trans. A* **1989**, *20*, 1933–1942. [[CrossRef](#)]

35. Momeni, A.; Dehghani, K. Prediction of Dynamic Recrystallization Kinetics and Grain Size for 410 Martensitic Stainless Steel during Hot Deformation. *Met. Mater. Int.* **2010**, *16*, 843–849. [[CrossRef](#)]
36. Lin, F.; Zhang, Y.; Tao, N.; Pantleon, W.; Juul Jensen, D. Effects of Heterogeneity on Recrystallization Kinetics of Nanocrystalline Copper Prepared by Dynamic Plastic Deformation. *Acta Mater.* **2014**, *72*, 252–261. [[CrossRef](#)]
37. Matsumoto, H.; Velay, V. Mesoscale Modeling of Dynamic Recrystallization Behavior, Grain Size Evolution, Dislocation Density, Processing Map Characteristic, and Room Temperature Strength of Ti-6Al-4V Alloy Forged in the (A+ β) Region. *J. Alloy. Compd.* **2017**, *708*, 404–413. [[CrossRef](#)]
38. Arun Babu, K.; Prithiv, T.S.; Gupta, A.; Mandal, S. Modeling and Simulation of Dynamic Recrystallization in Super Austenitic Stainless Steel Employing Combined Cellular Automaton, Artificial Neural Network and Finite Element Method. *Comput. Mater. Sci.* **2021**, *195*, 110482. [[CrossRef](#)]
39. Beltran, O.; Huang, K.; Logé, R.E. A Mean Field Model of Dynamic and Post-Dynamic Recrystallization Predicting Kinetics, Grain Size and Flow Stress. *Comput. Mater. Sci.* **2015**, *102*, 293–303. [[CrossRef](#)]
40. Zecevic, M.; Lebensohn, R.A.; McCabe, R.J.; Knezevic, M. Modelling Recrystallization Textures Driven by Intragranular Fluctuations Implemented in the Viscoplastic Self-Consistent Formulation. *Acta Mater.* **2019**, *164*, 530–546. [[CrossRef](#)]
41. Chuan, W.; He, Y.; Wei, L.H. Modeling of Discontinuous Dynamic Recrystallization of a Near- α Titanium Alloy IMI834 during Isothermal Hot Compression by Combining a Cellular Automaton Model with a Crystal Plasticity Finite Element Method. *Comput. Mater. Sci.* **2013**, *79*, 944–959. [[CrossRef](#)]
42. Zhao, P.; Wang, Y.; Niezgodna, S.R. Microstructural and Micromechanical Evolution during Dynamic Recrystallization. *Int. J. Plast.* **2018**, *100*, 52–68. [[CrossRef](#)]
43. Ruiz Sarrazola, D.A.; Pino Muñoz, D.; Bernacki, M. A New Numerical Framework for the Full Field Modeling of Dynamic Recrystallization in a CPFEM Context. *Comput. Mater. Sci.* **2020**, *179*, 109645. [[CrossRef](#)]
44. Yu, P.; Wu, C.; Shi, L. Analysis and Characterization of Dynamic Recrystallization and Grain Structure Evolution in Friction Stir Welding of Aluminum Plates. *Acta Mater.* **2021**, *207*, 116692. [[CrossRef](#)]
45. Raabe, D. Introduction of a Scalable Three-Dimensional Cellular Automaton with a Probabilistic Switching Rule for the Discrete Mesoscale Simulation of Recrystallization Phenomena. *Philos. Mag. A* **1999**, *79*, 2339–2358. [[CrossRef](#)]
46. Zhu, H.; Chen, F.; Zhang, H.; Cui, Z. Review on Modeling and Simulation of Microstructure Evolution during Dynamic Recrystallization Using Cellular Automaton Method. *Sci. China Technol. Sci.* **2020**, *63*, 357–396. [[CrossRef](#)]
47. Chang, K.; Chen, L.-Q.; Krill, C.E.; Moelans, N. Effect of Strong Nonuniformity in Grain Boundary Energy on 3-D Grain Growth Behavior: A Phase-Field Simulation Study. *Comput. Mater. Sci.* **2017**, *127*, 67–77. [[CrossRef](#)]
48. Maire, L.; Scholtes, B.; Moussa, C.; Bozzolo, N.; Muñoz, D.P.; Settefrati, A.; Bernacki, M. Modeling of Dynamic and Post-Dynamic Recrystallization by Coupling a Full Field Approach to Phenomenological Laws. *Mater. Des.* **2017**, *133*, 498–519. [[CrossRef](#)]
49. Mora, L.A.B.; Gottstein, G.; Shvindlerman, L.S. Three-Dimensional Grain Growth: Analytical Approaches and Computer Simulations. *Acta Mater.* **2008**, *56*, 5915–5926. [[CrossRef](#)]
50. Mellbin, Y.; Hallberg, H.; Ristinmaa, M. A Combined Crystal Plasticity and Graph-Based Vertex Model of Dynamic Recrystallization at Large Deformations. *Model. Simul. Mater. Sci. Eng.* **2015**, *23*, 045011. [[CrossRef](#)]
51. Glezer, A.M.; Kozlov, E.V.; Koneva, N.A.; Popova, N.A.; Kurzina, I.A. *Plastic Deformation of Nanostructured Materials*; CRC Press: Boca Raton, FL, USA, 2017; ISBN 978-1-315-11196-4.
52. Dyakonov, G.S.; Mironov, S.; Semenova, I.P.; Valiev, R.Z.; Semiatin, S.L. EBSD Analysis of Grain-Refinement Mechanisms Operating during Equal-Channel Angular Pressing of Commercial-Purity Titanium. *Acta Mater.* **2019**, *173*, 174–183. [[CrossRef](#)]
53. Hall, E.O. The Deformation and Ageing of Mild Steel: III Discussion of Results. *Proc. Phys. Soc. B* **1951**, *64*, 747–753. [[CrossRef](#)]
54. Petch, N.J. The Cleavage Strength of Polycrystals. *J. Iron Steel Inst.* **1953**, *174*, 25–28.
55. Armstrong, R.W. The Influence of Polycrystal Grain Size on Several Mechanical Properties of Materials. *Metall. Trans.* **1970**, *1*, 1169–1176. [[CrossRef](#)]
56. Knezevic, M.; Beyerlein, I.J. Multiscale Modeling of Microstructure-Property Relationships of Polycrystalline Metals during Thermo-Mechanical Deformation. *Adv. Eng. Mater.* **2018**, *20*, 1700956. [[CrossRef](#)]
57. Zhou, X.; Feng, Z.; Zhu, L.; Xu, J.; Miyagi, L.; Dong, H.; Sheng, H.; Wang, Y.; Li, Q.; Ma, Y.; et al. High-Pressure Strengthening in Ultrafine-Grained Metals. *Nature* **2020**, *579*, 67–72. [[CrossRef](#)] [[PubMed](#)]
58. Tan, J.C.; Tan, M.J. Superplasticity and Grain Boundary Sliding Characteristics in Two Stage Deformation of Mg-3Al-1Zn Alloy Sheet. *Mater. Sci. Eng. A* **2003**, *339*, 81–89. [[CrossRef](#)]
59. Quey, R.; Renversade, L. Optimal Polyhedral Description of 3D Polycrystals: Method and Application to Statistical and Synchrotron X-Ray Diffraction Data. *Comput. Methods Appl. Mech. Eng.* **2018**, *330*, 308–333. [[CrossRef](#)]
60. Roberts, W.; Boden, H.; Ahlblom, B. Dynamic Recrystallization Kinetics. *Metal. Sci.* **1979**, *13*, 195–205. [[CrossRef](#)]
61. Ponge, D.; Gottstein, G. Necklace Formation during Dynamic Recrystallization: Mechanisms and Impact on Flow Behavior. *Acta Mater.* **1998**, *46*, 69–80. [[CrossRef](#)]
62. Zurob, H.S.; Bréchet, Y.; Dunlop, J. Quantitative Criterion for Recrystallization Nucleation in Single-Phase Alloys: Prediction of Critical Strains and Incubation Times. *Acta Mater.* **2006**, *54*, 3983–3990. [[CrossRef](#)]
63. Cram, D.G.; Zurob, H.S.; Brechet, Y.J.M.; Hutchinson, C.R. Modelling Discontinuous Dynamic Recrystallization Using a Physically Based Model for Nucleation. *Acta Mater.* **2009**, *57*, 5218–5228. [[CrossRef](#)]

64. Beck, P.A.; Sperry, P.R. Strain Induced Grain Boundary Migration in High Purity Aluminum. *J. Appl. Phys.* **1950**, *21*, 150–152. [[CrossRef](#)]
65. Hallberg, H.; Wallin, M.; Ristinmaa, M. Simulation of Discontinuous Dynamic Recrystallization in Pure Cu Using a Probabilistic Cellular Automaton. *Comput. Mater. Sci.* **2010**, *49*, 25–34. [[CrossRef](#)]
66. Kondratev, N.S.; Trusov, P.V.; Podsedertsev, A.N. Multilevel model of polycrystals: Application to assessing the effect of texture and grains misorientation on the critical deformation of the dynamic recrystallization initiation. *PNRPU Mech. Bull.* **2021**, *4*, 83–97. (In Russian) [[CrossRef](#)]
67. Kondratev, N.S.; Trusov, P.V.; Podsedertsev, A.N. Multilevel physical-oriented model: Application to the description of the initial stage of dynamic recrystallization of polycrystals. *Probl. Strength Plast.* **2021**, *83*, 451–461. [[CrossRef](#)]
68. Lebensohn, R.A.; Brenner, R.; Castelnau, O.; Rollett, A.D. Orientation Image-Based Micromechanical Modelling of Subgrain Texture Evolution in Polycrystalline Copper. *Acta Mater.* **2008**, *56*, 3914–3926. [[CrossRef](#)]
69. Kondratev, N.S.; Trusov, P.V. Description of Hardening Slip Systems Due to the Boundaries of the Crystallites in a Polycrystalline Aggregate. *PNRPU Mech. Bull.* **2012**, *3*, 78–97. (In Russian)
70. Trusov, P.V.; Shveykin, A.I. On Motion Decomposition and Constitutive Relations in Geometrically Nonlinear Elastoviscoplasticity of Crystallites. *Phys. Mesomech.* **2017**, *20*, 377–391. [[CrossRef](#)]
71. Anand, L. Single-Crystal Elasto-Viscoplasticity: Application to Texture Evolution in Polycrystalline Metals at Large Strains. *Comput. Methods Appl. Mech. Eng.* **2004**, *193*, 5359–5383. [[CrossRef](#)]
72. Bronkhorst, C.A.; Kalidindi, S.R.; Anand, L. Polycrystalline Plasticity and the Evolution of Crystallographic Texture in FCC Metals. *Phil. Trans. R. Soc. Lond. A* **1992**, *341*, 443–477. [[CrossRef](#)]
73. Bailey, J.E.; Hirsch, P.B. The Recrystallization Process in Some Polycrystalline Metals. In *Proceedings of the Royal Society of London. Series, A. Mathematical and Physical Sciences*; The Royal Society: London, UK, 1962; Volume 267, pp. 11–30. [[CrossRef](#)]
74. Mitchell, M. *An Introduction to Genetic Algorithms*; MIT Press: Massachusetts, USA, 1998; ISBN 978-0-262-63185-3.
75. Pozdeev, A.A.; Trusov, P.V.; Nyashin, Y.I. *Large Elastoplastic Deformations: Theory, Algorithms, Applications*; Nauka: Moscow, Russia, 1986. (In Russian)
76. Chang, Y.A.; Himmel, L. Temperature Dependence of the Elastic Constants of Cu, Ag, and Au above Room Temperature. *J. Appl. Phys.* **1966**, *37*, 3567–3572. [[CrossRef](#)]
77. Ledbetter, H.M.; Naimon, E.R. Elastic Properties of Metals and Alloys. II. Copper. *J. Phys. Chem. Ref. Data* **1974**, *3*, 897–935. [[CrossRef](#)]
78. Blaz, L.; Sakai, T.; Jonas, J.J. Effect of Initial Grain Size on Dynamic Recrystallization of Copper. *Metal Sci.* **1983**, *17*, 609–616. [[CrossRef](#)]
79. Kondratev, N.S.; Trusov, P.V.; Podsedertsev, A.N. The polycrystals grain structure formation for modified two-level crystal plasticity statistical models. *Procedia Struct. Integr.* **2022**, *in press*.
80. Vaz, M.F.; Fortes, M.A. Grain Size Distribution: The Lognormal and the Gamma Distribution Functions. *Scr. Metall.* **1988**, *22*, 35–40. [[CrossRef](#)]
81. Raeisina, B.; Sinclair, C.W. A Representative Grain Size for the Mechanical Response of Polycrystals. *Mater. Sci. Eng. A* **2009**, *525*, 78–82. [[CrossRef](#)]
82. Kondratev, N.S.; Trusov, P.V. To Determination a Distribution Law of Subgrain Sizes Formed in the Cold Plastic Deformation Process. *AIP Conf. Proc.* **2020**, *2216*, 040010. [[CrossRef](#)]
83. Suresh, K.S.; Rollett, A.D.; Suwas, S. Evolution of Microstructure and Texture During Deformation and Recrystallization of Heavily Rolled Cu-Cu Multilayer. *Metall. Mater. Trans. A* **2013**, *44*, 3866–3881. [[CrossRef](#)]